Chapter 4

Results and Discussion

In this Chapter, we will present the experiment results and the corresponding discussion. As will be seen in the following, there are two types of tunnel junctions to be measured, Al/AlO_x/Sc and Al/AlO_x/Al. Although the measurement circuits have been described in detailed in Chapter 3, we remind ourself here by a sketch as shown in Fig. 4.1, which shows the bias polarity of the junction under measuring. For the Al/AlO_x/Sc junctions, we applied the bias V to the Sc lead while treat the Al lead as ground, and for the Al/AlO_x/Al junctions, we applied the bias V to the second evaporated Al lead while treat the first evaporated Al lead as ground.

4.1 The Quality, Height, and Thickness of the Barrier

4.1.1 The Quality of the Barrier

The control of the thickness of the barrier in the M-I-M tunnel junction is crucial to fabricate a tunnel junction which is suitable for measurement. The thicker the barrier, the larger the resistance of the junction, and therefore the larger the

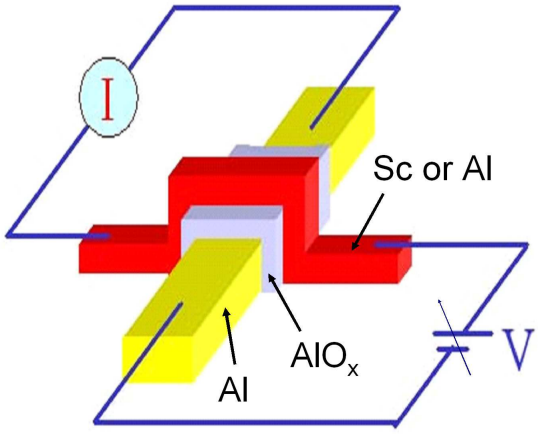

Figure 4.1: The bias polarity in the tunnel junctions under measurement.

(Johnson) noise in the measurement. So, it seems reasonable to grow a barrier as thinner as possible. But, the thinner the barrier, the higher the probability of the existence of pinholes which will lead to leakage current so that the conduction mechanism through the junction is not only electron tunneling. There are several criteria widely used to ascertain a good tunnel junction (a good tunnel junction means that the electron tunneling is the dominate conduction mechanism)[36, 37]: (i) an exponential barrier thickness (t) dependence of the conductance, $G(t) \sim \exp(2t/t_0)$, with $t_0 = \hbar/2\sqrt{2m\phi}$ (where m is the electron mass and ϕ is the barrier height), (ii) a parabolic voltage (V) dependence of the conductance $G(V)$ that can be fitted to theoretical models as mentioned in chapter 2, (iii) an insulating-like temperature dependence of the junction resistance at zero-bias, and (iv) using a superconductor as one lead of the junction, and measuring the superconducting gap below its T_C.

Since we grew the insulating layer by oxidizing the Al films (glow discharge in an dilute O_2 atmosphere), the oxidation rate is sensitive to the strength of the electric

field the Al films suffered. In our setup, the oxidation rate depends on the position of the Al films. So criterion (i), which is based on the assumption that the oxidation rate is the same everywhere, is not applicable to our case. The validity of criterion (ii) and (iii) is based on the condition that both the two leads in the junction are free-electron metals and there is no additional interaction exerted on the tunneling electrons except the influence of the barrier. In our Al/AlO_x/Sc tunnel junctions, we found there existed interaction exerted on the electrons when they tunnel through the barrier, so criterion (ii) and (iii) are not applicable to our case. Therefore, the only reliable criterion is criterion (iv), which was proposed by Giaever [37], who mentioned that this is the only test of tunneling in a junction.

Before time and effort are expended in taking the data which we are interested in, we test the criterion (iv) first. We usually run the ^{3}He fridge to its base temperature ($\sim$ 250 mK), and measure the dI/dV using the "send V measure I" circuit as shown in Fig. **??**. Since the T_C of the Al films in our tunnel junctions is about 2 K, and the Sc films maintain their normal metal state at least down to 250 mK, therefore at the base temperature, Al films are in superconducting state and Sc films are in normal metal state. The measurement reveals a good BCS superconduction gap as shown in Fig. 4.2. In Fig. 4.2, we observe an energy gap $E_g(0.248\ \mathrm{K}) = 2\Delta(0.248\ \mathrm{K}) \approx 0.6$ meV ($\Delta(0.248\ \mathrm{K}) \approx 0.3$ meV). On the other hand, from measuring the resistance of the Al film as a function of temperature, we can get $T_C \approx 1.95$ K which can be seen in the inset in Fig. 4.2. According to BCS theory, for the superconductor with this T_C value, $\Delta_{BCS}(0.248\ \mathrm{K}) \approx \Delta_{BCS}(0) = 1.764 k_B T_C \approx 0.3$ meV, and this is in agreement with the result we observed. The zero-bias conductance of the junction as the Al film is in normal state is approximately equal to the conductance at bias which is

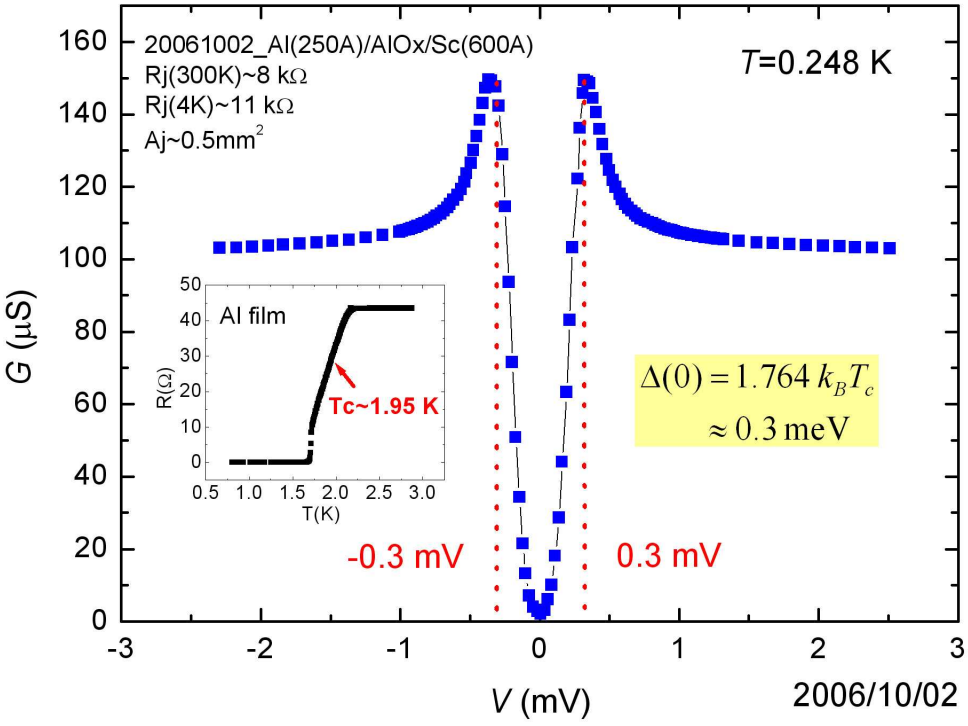

Figure 4.2: The superconducting gap of the Al film.
The measurement was done at 248 mK, which is below the critical temperature T_c ($\approx$ 1.95 K) of the Al film . The spectrum shows a good BCS superconducting gap. Inset: The resistance of the Al film as a function of temperature shows a superconducting transition at $T \approx 1.95$ K.

larger than one half of the gap whether the Al film is in its superconducting state or not, i.e. $G(0, T > T_C) \approx G(V', T)|_{eV'>\Delta}$, where 2Δ is the superconducting gap. From Fig. 4.2, the ratio of the zero-bias conductance as Al film is in superconducting state to that as it is in normal state is

$$\frac{G(0, T < T_C)}{G(0, T > T_C)} \approx \frac{G(0, T < T_C)}{G(V', T)|_{eV'>\Delta}} \approx 0.01, \tag{4.1}$$

here we choose $V' \approx -2.3$ mV. Although theoretically, for a pinhole free junction, the ratio defined above as $T \to 0$ is 0, in a realistic situation, the ratio obtained from experiments is not 0. This is due to the finite temperature effect and for the most part due to the resolution ability of the measurement circuits, especially for the small gap superconductor. In the worst case, if the obtained non-zero ratio is not due to the resolution limit, but is really due to the existence of pinholes, it can be said that the conductance through the pinholes contributes $\approx 1\%$ to the total conductance and can be neglected. Therefore, we can demonstrate the dominant conduction mechanism through the junction is electron tunneling.

It is instructive to inspect the temperature dependence of the zero-bias conductance of the junction. As shown in Fig. 4.3, the temperature dependence can be divided into 2 regimes. In regime I, the conductance decreases as temperature decreases from ∼300 K to ∼50 K, which reveals an insulating behavior, and this is in agreements with criterion (iii). In regime II, some thing interesting occurs. The conductance increases as temperature decreases from ∼ 50 K to ∼ 2.5 K, and this contracts to criterion (iii). We should note that the anomalies in regime II is not due to the bad quality of the barrier according to the superconducting gap measurement mentioned above, but is due that there exists an additional interaction exerted on the electrons when they tunnel through the barrier. The details of the anomalies

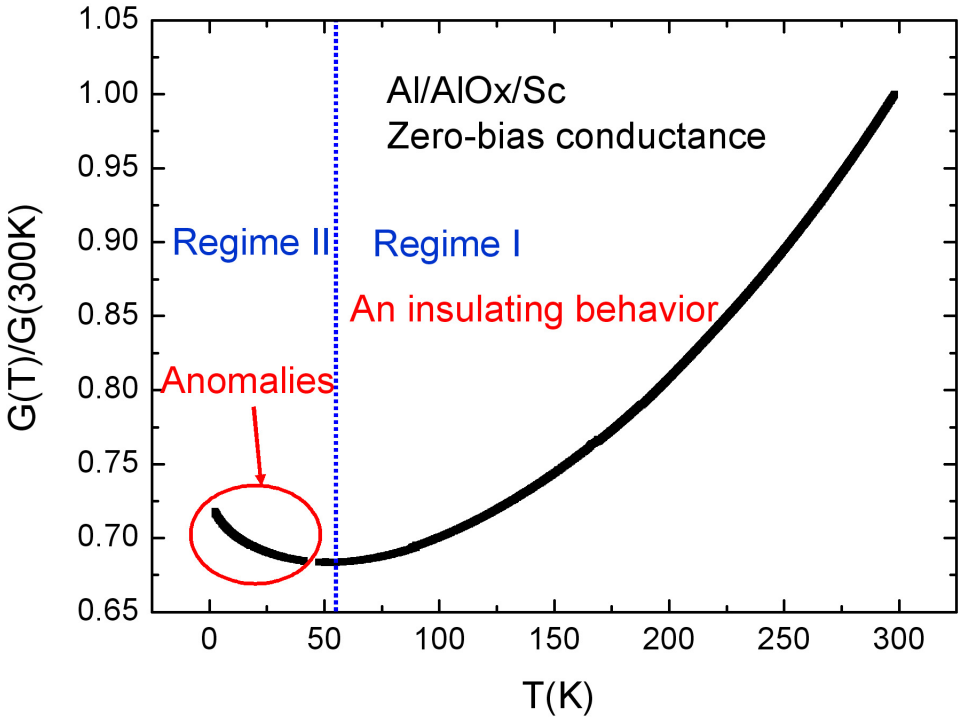

Figure 4.3: The zero-bias conductance $G(0,T)$ as a function of temperature. In regime I, the conductance decreases as temperature decreases, which behaves like an insulator. In regime II, the conductance increases as temperature decreases, which is due to the spin-spin interactions exerted on the tunneling electrons.

will be discussed later.

4.1.2 The Height and Thickness of the Barrier

We have demonstrated that the dominant conduction mechanism in these $Al/AlO_x/Sc$ junctions is electron tunneling. And now we ask a question: What is the values of the barrier height and thickness? As mentioned in chapter 2, the BDR model can be utilized to determine the height and thickness of the barrier in a tunnel junction if both the two leads in a tunnel junction are free-electron metals and there is no additional interaction exerted on the tunneling electrons. In these $Al/AlO_x/Sc$ tunnel junctions, the tunneling electrons suffer spin-spin interactions (which will be discussed later), so the BDR model is not applicable to these junctions.

To know the barrier parameters we have another idea: The thickness of the barrier should depend only on the parameters (e.g. the power of the plasma, the flux of the O_2 gas, and the steady-state pressure, etc.) which we used in the glow discharge process. If we use the same parameters which are used in fabricating the barrier of $Al/AlO_x/Sc$ junctions to make the barrier of $Al/AlO_x/Al$ junctions, the barrier thickness in these two types of junctions should be the same. Therefore, we fabricated several $Al/AlO_x/Al$ junctions using the same glow discharge parameters as used in fabricating $Al/AlO_x/Sc$ junctions, and measured the differential conductance spectra in these $Al/AlO_x/Al$ junctions. The barrier parameters can be obtained by least-square fittings of the data using BDR model which includes the thermal effect, (2.39). We treat $G(0,T)$, A_0, $\Delta\phi$, and $\bar{\phi}$ in (2.39) as free parameters in the fitting procedures. After obtaining these parameters, the barrier height from lead 1, ϕ_1, from lead 2, ϕ_2, and the barrier thickness, t, can be determined by (2.31),

(2.32), and (2.33).

Fig. 4.4 shows the results of fitting. Fig. 4.4 (a) shows a junction whose cross section $\approx$ 0.4 mm^2 measured at 5 K. The fitted parameters are $\phi_1 \approx 1.88$ eV, $\phi_2 \approx 0.4$ eV, $\bar{\phi} \approx 1.14$ eV, and $t \approx 16.9$ Å. Fig. 4.4 (b) shows a junction whose cross section ≈ 0.5 mm^2 measured at 299 K. The fitted parameters are $\phi_1 \approx 2.78$ eV, $\phi_2 \approx 0.6$ eV, $\bar{\phi} \approx 1.69$ eV, and $t \approx 18.8$ Å. Inspecting these results, we find the fitted $\bar{\phi}$ and t in the 0.4 mm^2 junction are smaller than that in the 0.5 mm^2 junction, and by intuition, it seems to imply the conductance per unit cross section area, G/R_j, in the former is larger than that in the latter at the same temperature. Indeed it is the case, since the $G(300\text{K})/R_j$ in the former $\approx 500\mu$S/mm^2 is larger than that in the latter $\approx 400\mu$S/mm^2, and this is consistent with the fitting results. The theoretical model describes the experimental data well in both these two junctions as shown in Fig. 4.4. We believe the barrier thickness obtained in these Al/AlO$_x$/Al junctions is close to that in Al/AlO$_x$/Sc junctions since we using the same glow discharge parameters. But the barrier height in these two types of junctions may be different due to the work functions of Al and of Sc are unequal.

4.2 Differential Conductance in Al/AlO$_x$/Sc Tunnel Junctions

4.2.1 $G(0,T)$ vs. T

Now we return to the data in Al/AlO$_x$/Sc junctions. As shown in Fig. 4.3, the zero-bias conductance increases as temperature decreases between $T \sim 50$ K and $T \sim 2.5$ K, which contracts to the insulating-like behavior in the high temperature regime. The anomalies are not due to the bad quality of the barrier which has been

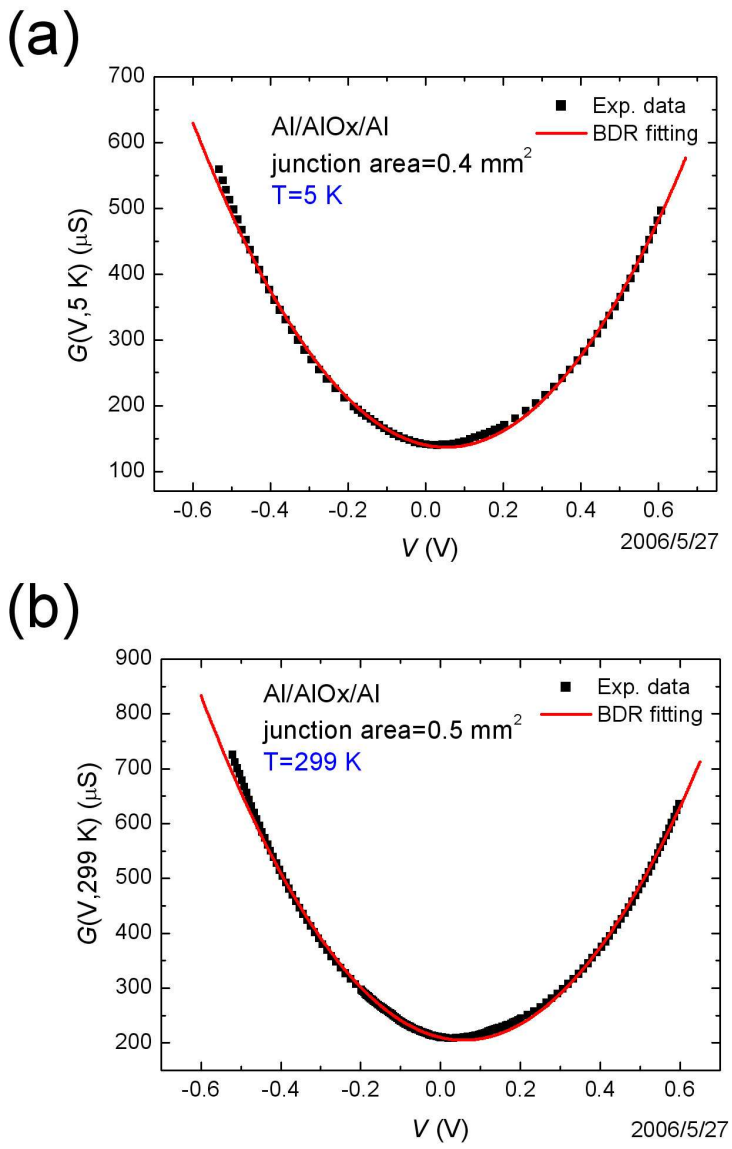

Figure 4.4: The $G(V,T)$ spectra of two $Al/AlO_x/Al$ junctions. Symbols are the experimental data and curves are the theoretical fitting. (a) T=5 K, and the junction area $\approx$ 0.4 mm^2. The fitted parameters are $\phi_1 \approx 1.88$ eV, $\phi_2 \approx 0.4$ eV, $\bar{\phi} \approx 1.14$ eV, and $t \approx 16.9$ Å. (b) $T = 299$ K, and the junction area ≈ 0.5 mm^2. The fitted parameters are $\phi_1 \approx 2.78$ eV, $\phi_2 \approx 0.6$ eV, $\bar{\phi} \approx 1.69$ eV, and $t \approx 18.8$ Å.

demonstrated by the measurement of the superconducting gap of the Al film, but are really due to some interesting conduction mechanism.

If we plot $G(0,T)$ as a function of T using a log$T$ scale for $T \lesssim 50$ K, as shown in Fig. 4.5, we will find the absorbing behavior: $G(0,T)$ reveals a $-\log T$ dependence for 16 K $\lesssim T \lesssim$ 32 K, and starts to deviate from the $-\log T$ dependence as $T \lesssim 16$ K. The lower the temperature, the larger the deviation, and $G(0,T)$ gradually saturates at low temperatures.

4.2.2 $G(V,T)$ vs. V

We have seen the anomalies in $G(0,T)$ as a function of temperature for $T \lesssim 32$ K, and now we turn to $G(V,T)$ as a function of V. The $G(V,T)$ spectra for two Al/AlO_x/Sc junctions are shown in Fig. 4.6 and in Fig. 4.7, respectively. We see, in Fig. 4.6, at 300 K, $G(V, 300\text{ K})$ behaves like a parabola, and the magnitudes of the parabola decreases as temperature decreases. As $T \lesssim 32$ K, some thing interesting appears: a conductance peak occurs around zero-bias, and the lower the temperature, the higher the peak and the narrower the width of the peak, which can be seen in Fig. 4.6 and in Fig. 4.7. This is consistent with the $G(0,T)$ behavior described above.

What is the reason for the anomalies? We know, according to (2.58)$\sim$(2.71), the measured $G(V,T)$ spectra should contain the information of the correction of the DOS in both the leads of a tunnel junction and of the tunneling rate (the transition rate) due to the additional interaction exerted on the tunneling electrons. The evaporated leads, Al films and Sc films, will have certain degree of disorder, and strictly speaking, are not free-electron metals. According to Altshuler's theory [38], for a

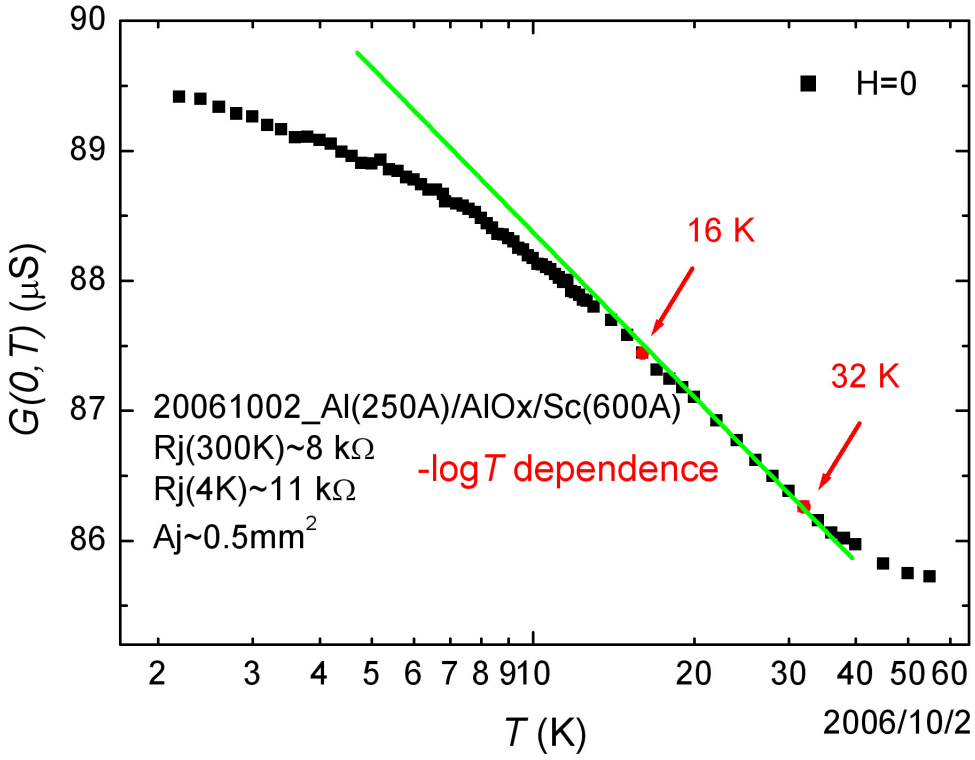

Figure 4.5: $G(0,T)$ as a function of temperature for $T \lesssim 50$ K. The temperature is in a log scale. Symbols are the experimental data and the line is guided to eyes. $G(0,T) = a - b \log T$ for 14 K $\lesssim T \lesssim$ 32 K, and $G(0,T)$ starts to deviate the $-\log T$ dependence as $T \lesssim 14$ K.

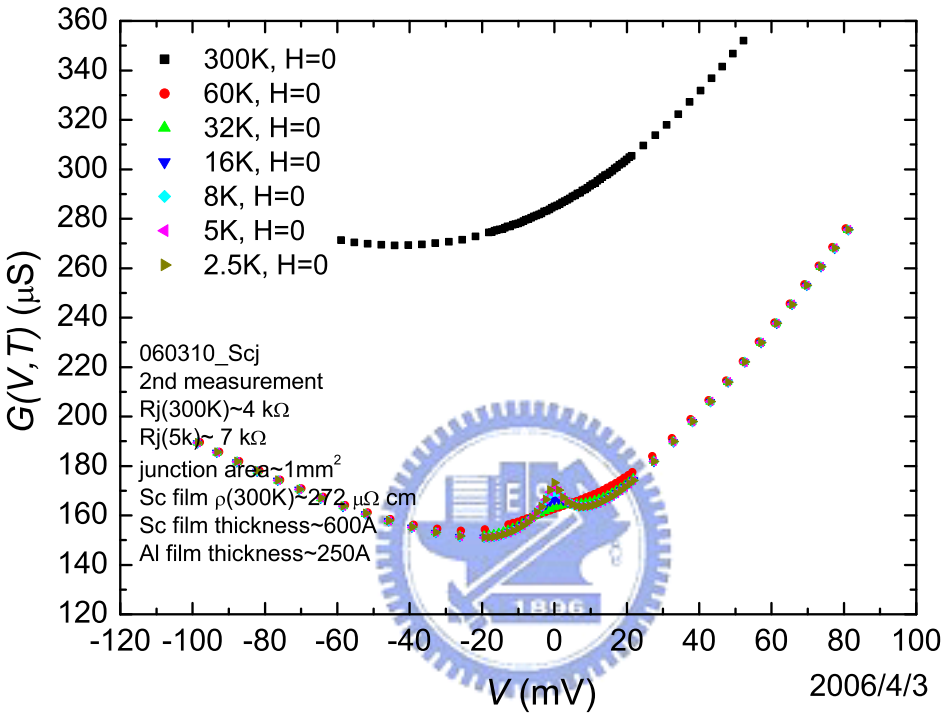

Figure 4.6: $G(V,T)$ as a function of V at several temperatures of a Al/AlO$_x$/Sc tunnel junction.
At 300 K, the $G(V, 300\text{ K})$ spectrum is like a parabola which can be explained by BDR model. The magnitudes of the parabola decreases as temperatures decreases, but as $T \lesssim 32$ K, a conductance peak occurs around zero-bias. The lower the temperature, the higher the peak and the narrower the width of the peak.

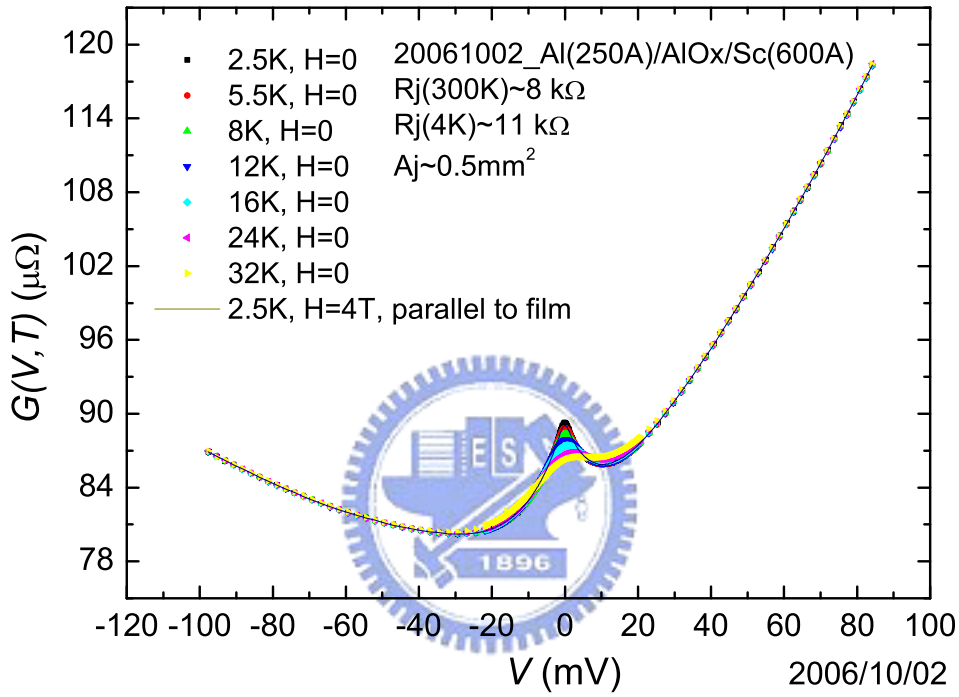

Figure 4.7: $G(V,T)$ as a function of V for several temperatures of another $Al/AlO_x/Sc$ tunnel junction
The $G(V,T)$ spectra of this junction are similar to that in another junction as shown in Fig. 4.6.

disordered metal, the density of states around Fermi energy will be suppressed by the enhanced electron-electron interaction due to the disorder. The suppression of DOS will cause a conductance dip around zero-bias in the $G(V,T)$ spectra, and this contradicts our result of conductance peak. On the other hand, the conductance peak is not concerned in the Al film. This is obvious since we observe the conductance dip in Al/AlO_x/Al tunnel junctions as shown in Fig. 4.9 and Fig. 4.11. Therefore we think the conductance peak is due to the additional interaction exerted on the electrons and enhancing their tunneling. The existence of the interaction must be related to the Sc film.

Since the electronic configuration of a Sc atom is $[Ar]3d^14s^2$, the spin angular momentum of a single Sc atom is 1/2. In the fabrication process, some Sc atoms may diffuse into the barrier to form localized spins. We therefore conjecture that there maybe exists the free electron-localized spin interaction which is exerted on electrons as they tunnel through the barrier. The $-\log T$ dependence of $G(0,T)$ and the zero-bias peak of $G(V,T)$ in Al/AlO_x/Sc junctions at low temperatures should be due to this interaction. If this is really the case, Appelbaum's theory [2], which considers the $s-d$ exchange interaction between the tunneling electrons and the localized spins in the barrier, should be able to describe our experimental results.

Since the measured $G(V,T)$ spectra contain the information of the correction of the DOS in both the leads of a tunnel junction, we should discuss the degree of correction in DOS of the Al and Sc film before analyze the free electron-localized spin interaction.

4.3 The DOS Effects in the Al and Sc Leads

4.3.1 The DOS Effect in the Al Lead

First, we consider the DOS effect in the first evaporated Al films. Although we should make the first evaporated Al film to be a free-electron metal as possible as we can (to reduced the DOS effect), in practice, the evaporated film still has certain degree of disorder, and whose resistivity at room temperature is ~ 15 $\mu\Omega$ cm. How much is the contribution due to the disorder of the first evaporated Al film to the differential conductance?

To answer this question, we fabricated several Al/AlO_x/Al tunnel junctions and intentionally let the degree of disorder in the second evaporated Al film be the same with that in the first evaporated one (using the same evaporation parameters), i.e. we fabricated several Al (15 $\mu\Omega$ cm)/AlO_x/Al (15 $\mu\Omega$ cm) tunnel junctions. Then we measured their differential conductance at low temperatures. Fig. 4.8 shows the resistivity of the last evaporated Al film as a function of temperature. We note the residual resistivity ratio (RRR, which is defined as the ratio of the resistivity at room temperature to the residual resistivity) is ~ 1.2. The value of the RRR can be used to characterize the degree of disorder in a metal. The larger the value, the less the degree of disorder. Fig. 4.9 shows the $G(V,T)$ in this Al (15 $\mu\Omega$ cm)/AlO_x/Al (15 $\mu\Omega$ cm) tunnel junction. We find the suppression occurs around zero-bias as $T \lesssim 8$ K, and at $T \sim 3$ K, the suppression is $\sim 1/1000$ compared to the parabolic background (for large bias range, the spectra are similar to that in Fig. 4.4). Since there is no additional interaction exerted on the tunneling electrons in Al/AlO_x/Al junctions, the measured $G(V,T)$ should be described by (2.69), and at zero bias, the

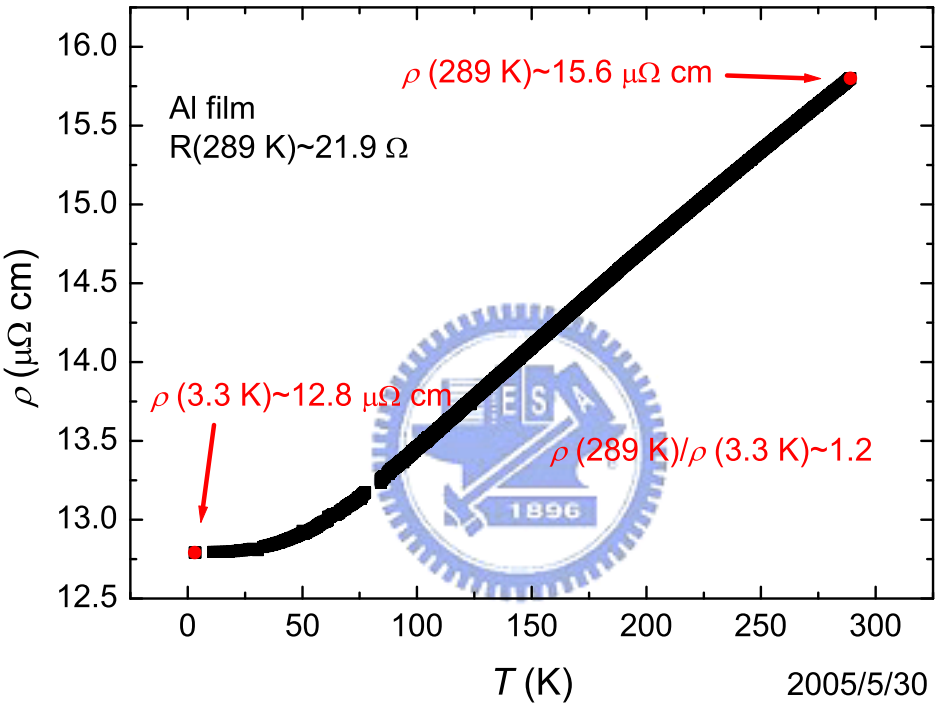

Figure 4.8: $\rho(T)$ vs. T for an Al film whose $\rho(300\ \mathrm{K}) \approx 15.6\ \mu\Omega$ cm.

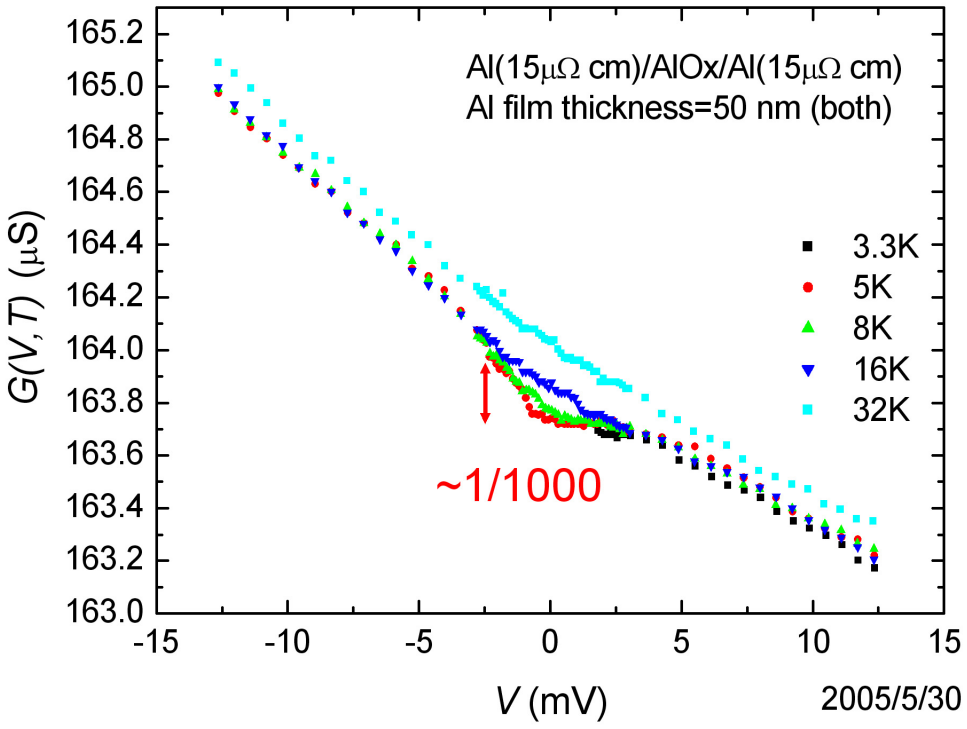

Figure 4.9: The $G(V,T)$ spectra of an Al (15 $\mu\Omega$ cm)/AlO_x/Al (15 $\mu\Omega$ cm) tunnel junction.
The conductance suppression occurs around zero-bias as $T \lesssim 8$ K, and at $T \sim 3$ K, the suppression is $\sim 1/1000$ compared to the parabolic background.

conductance

$$\begin{aligned} G(0) &\approx G^B_{free}(0) + 2e^2 P^{B,1st} N^0_1(0)\Delta N_2(0) \\ &\quad +2e^2 P^{B,1st}\Delta N_1(0) N^0_2(0). \end{aligned} \tag{4.2}$$

where

$$\begin{aligned} G^B_{free}(0) &\equiv \frac{\partial[J^B_{free}(V)|_{V\to 0}]}{\partial V} \\ &= \frac{\partial[2eP^{B,1st}N^0_1(0)N^0_2(0)eV]}{\partial V} \\ &= 2e^2 P^{B,1st} N^0_1(0) N^0_2(0). \end{aligned} \tag{4.3}$$

Substitute (4.3) into (4.2), we obtain

$$\begin{aligned} G(0) &\approx 2e^2 P^{B,1st} N^0_1(0) N^0_2(0) + 2e^2 P^{B,1st} N^0_1(0)\Delta N_2(0) \\ &\quad +2e^2 P^{B,1st}\Delta N_1(0) N^0_2(0) \\ &= 2e^2 P^{B,1st} N^0_1(0) N^0_2(0)[1 + \frac{\Delta N_2(0)}{N^0_2(0)} + \frac{\Delta N_1(0)}{N^0_1(0)}] \qquad (4.4) \\ &= 2e^2 P^{B,1st} N^0_1(0) N^0_2(0)[1 + 2\frac{\Delta N_1(0)}{N^0_1(0)}]. \qquad (4.5) \end{aligned}$$

To get (4.5), we use the relations $N^0_1(0) = N^0_2(0)$ and $\Delta N_1(0) = \Delta N_2(0)$ due the the same metal leads and the same degree of disorder in the Al(15 $\mu\Omega$ cm)/AlO_x/Al(15 $\mu\Omega$ cm) tunnel junction. Comparing (4.5) with Fig. 4.9, we estimate $\Delta N_1(0)/N^0_1(0)$ is of the order $\sim 1/1000$, and therefore $\Delta N_1(\epsilon)/N^0_1(\epsilon)$
$\lesssim 1/1000$ if $\epsilon \neq 0$ since the maximum of the the conductance suppression occurs at zero-bias.

Now if we increase the degree of disorder in the last evaporated Al film, how does this affect $G(V,T)$? We fabricated several Al(15 $\mu\Omega$ cm)/AlO_x/Al

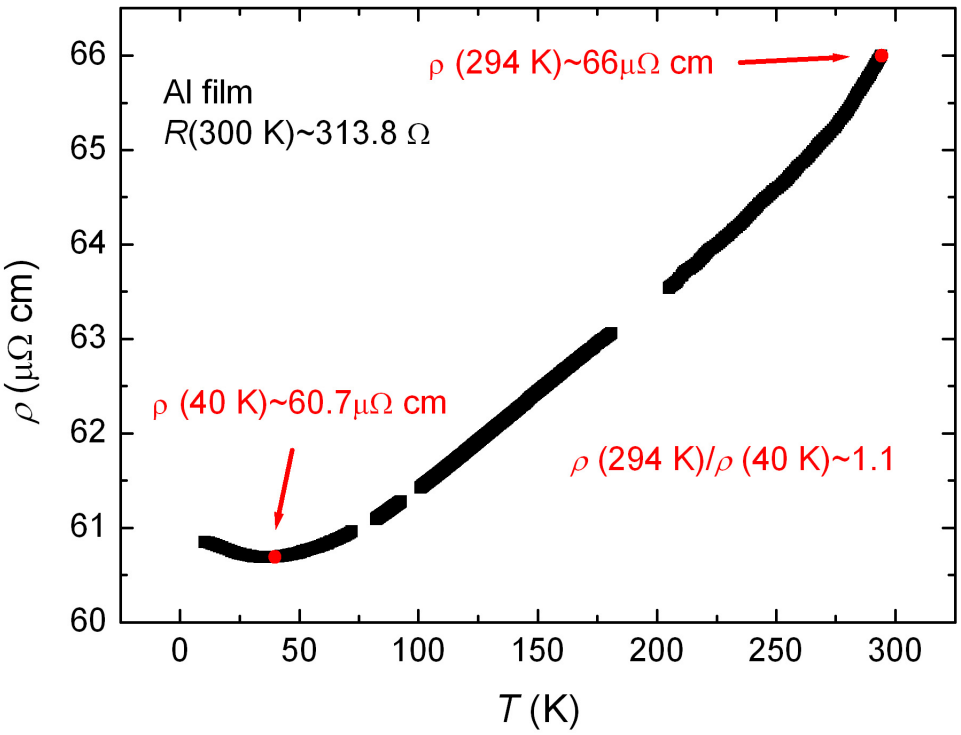

Figure 4.10: $\rho(T)$ vs. T for an Al film whose $\rho(300\ \mathrm{K}) \approx 66\ \mu\Omega$ cm .

(66 $\mu\Omega$ cm) junctions and did the measurement. Fig. 4.10 shows the resistivity as a function of temperature of the last evaporated Al film whose resistivity at room temperature is $\sim$ 66 $\mu\Omega$ cm, and the RRR in this film is $\sim$ 1.1. Fig. 4.11 shows the $G(V,T)$ spectra in such a junction. Note the suppression of the conductance around zero-bias, at $T \sim 5.3$ K, is $\sim 1/100$ compared to the parabolic background. Comparing this with (4.4), and using $\Delta N_1(0)/N_1^0(0) \sim 1/1000$, we estimate $\Delta N_2(0)/N_2^0(0) \sim 1/100$. From these experiments, we find that the higher the degree of disorder (the lower RRR value), the more the suppression in the density of states, which is consistent with the theoretical prediction.

4.3.2 The DOS Effect in the Sc Lead

Now we consider the density of states effect in the Sc film. From Fig. 4.6 or Fig. 4.7, it is hard to extract the information of DOS in the Sc film through the $G(V,T)$ spectra in Al/AlO_x/Sc since the spectra contain the information of both the DOS effect and the additional interaction. But according to the RRR value in the Sc film, we can make an estimation. Fig. 4.12 shows the resistivity of a Sc film as a function of temperature. Note that the RRR is ~ 2 and this is greater than that in the first evaporated Al films (~ 1.2) mentioned above. Therefore it is reasonable to estimate the suppression of DOS in the Sc films to be less than that in the Al films. We estimate the maximum of the suppression of DOS in these Sc films is $\sim 1/1000$, i.e. $\Delta N_{Sc}(\epsilon)/N_{Sc}^0(\epsilon) \lesssim 1/1000$. Therefore, according to (2.58) $\sim$ (2.67), in these Al/AlO_x/Sc tunnel junctions, the net tunneling current, as $T \to 0$, is

$$\begin{aligned} J(V) &= J^B_{free}(V) + J^B_{\Delta N_{Sc}}(V) + J^B_{\Delta N_{Al}}(V) + J^B_{\Delta N_{Al},\Delta N_{Sc}}(V) \\ &\quad + J^{Int}_{free}(V) + J^{Int}_{\Delta N_{Sc}}(V) + J^{Int}_{\Delta N_{Al}}(V) + J^{Int}_{\Delta N_{Al},\Delta N_{Sc}}(V) \end{aligned}$$

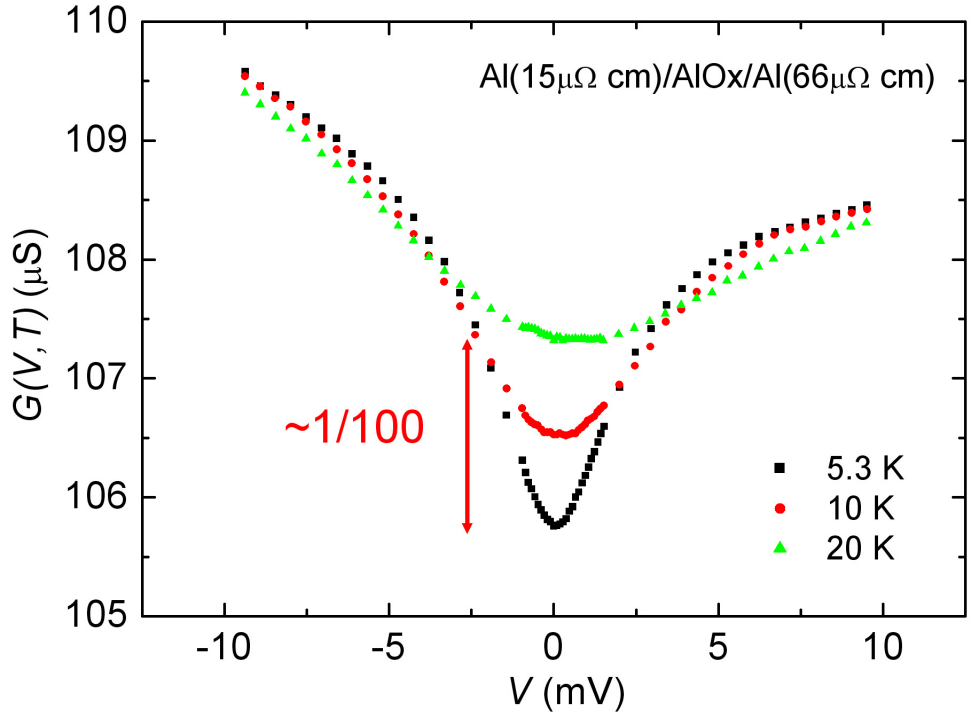

Figure 4.11: The $G(V,T)$ spectra of an Al (15 $\mu\Omega$ cm)/AlO_x/Al (66 $\mu\Omega$ cm) tunnel junction.
The suppression of the conductance around zero-bias, at $T \sim 5.3$ K, is $\sim 1/100$ compared to the parabolic background.

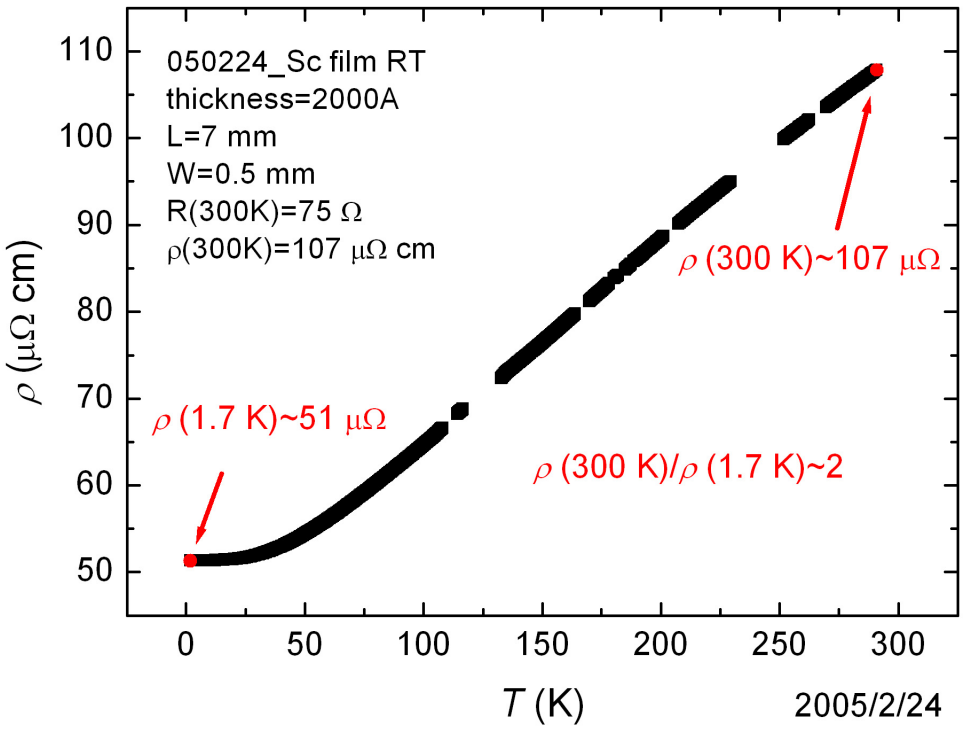

Figure 4.12: $\rho(T)$ vs. T for a Sc film whose $\rho(300\ \mathrm{K}) \approx 107\ \mu\Omega$ cm.

$$\approx \quad J^B_{free}(V) + J^B_{\Delta N_{Sc}}(V) + J^B_{\Delta N_{Al}}(V) + J^{Int}_{free}(V) + J^{Int}_{\Delta N_{Sc}}(V) + J^{Int}_{\Delta N_{Al}}(V), \tag{4.6}$$

where we neglected the second order of the DOS correction ($\Delta N_{Al}\Delta N_{Sc}$). Since $\Delta N_{Al}(\epsilon)/N^0_{Al}(\epsilon) \lesssim 1/1000$ and $\Delta N_{Sc}(\epsilon)/N^0_{Sc}(\epsilon) \lesssim 1/1000$, we have $J^B_{\Delta N_{Sc}}(V) << J^B_{free}(V)$, $J^B_{\Delta N_{Al}}(V) << J^B_{free}(V)$, $J^{Int}_{\Delta N_{Sc}}(V) << J^{Int}_{free}(V)$, and $J^{Int}_{\Delta N_{Al}}(V) << J^{Int}_{free}(V)$ according to (2.60) $\sim$ (2.67). So, (4.6) can be reduced to

$$J(V) \approx J^B_{free}(V) + J^{Int}_{free}(V), \tag{4.7}$$

and therefore

$$G(V) \approx G^B_{free}(V) + G^{Int}_{free}(V), \tag{4.8}$$

It means that, in these Al/AlO_x/Sc tunnel junctions, the $G(V,T)$ spectra can be approximately viewed as the superposition of the conductance due to the additional interaction, $G^{Int}_{free}(V)$, and the conductance due the tunneling between two free-electron metals, $G^B_{free}(V)$, which has been described in (2.71).

4.4 Subtracting the Background from the Measured dI/dV Data

The original data we obtained from the dI/dV measurement contain the contributions of the normal tunneling due to the barrier (tunneling between two free-electron metals) and of the enhanced tunneling due to the $s-d$ exchange interaction (the additional interaction). To obtain the signal contributed from the $s-d$ exchange interaction, the signal from the normal tunneling should be subtracted from the original data. According to BDR model, the normal tunneling conductance, $G^B_{free}(V)$,

should be a parabolic function of bias V, as mentioned in chapter 2. Therefore, to get the conductance contributed from the $s-d$ exchange interaction, we should subtract the parabolic background from the originally measured $G(V,T)$ data.

Here we analyze the data of one of these Al/AlO_x/Sc tunnel junctions, namely "20061002_Al/AlO_x/Sc", whose $G(V,T)$ spectra have been shown in Fig. 4.7. We emphasize that all our measured Al/AlO_x/Sc junctions have the similar behavior. Fig. 4.13 is enlarged from Fig. 4.7 for -20 mV $\lesssim V \lesssim$ 20 mV. We tried plotting a *suitable* parabolic background as shown in Fig. 4.13. Since the measured $G(V,T)$ spectra are contributed from not only the normal tunneling but also the additional interaction exerted on the tunneling electrons, it is hard to determine the *real* background, i.e., the contribution of the normal tunneling only. The parabolic background we choose is guided to eyes, and may differ from the real background with an offset. Since in the fitting process, the offset can be absorbed into the constant A in (2.144), the existence of the offset will not affect the fact that if the theory can describe the data.

After subtracting the background, $G_{remainder}(V,T)$ is obtained as shown in Fig. 4.14. We find in Fig. 4.14, $G_{remainder}$ is not symmetric to $V=0$, and therefore it must contain an asymmetric term. According to Appelbaum's calculation, the conductance due to the $s-d$ interaction, $G_2(V)+G_3(V)$, is an even function, i.e., it is symmetric to $V=0$, which can be seen from (2.140), (2.141), and (2.142). The even function proof is left in appendix A. Therefore, we should divide the $G_{remainder}$ data into an even and an odd part. They are defined as

$$G_{even,data}(V,T) \equiv \frac{G_{remainder}(V,T)+G_{remainder}(-V,T)}{2}, \tag{4.9}$$

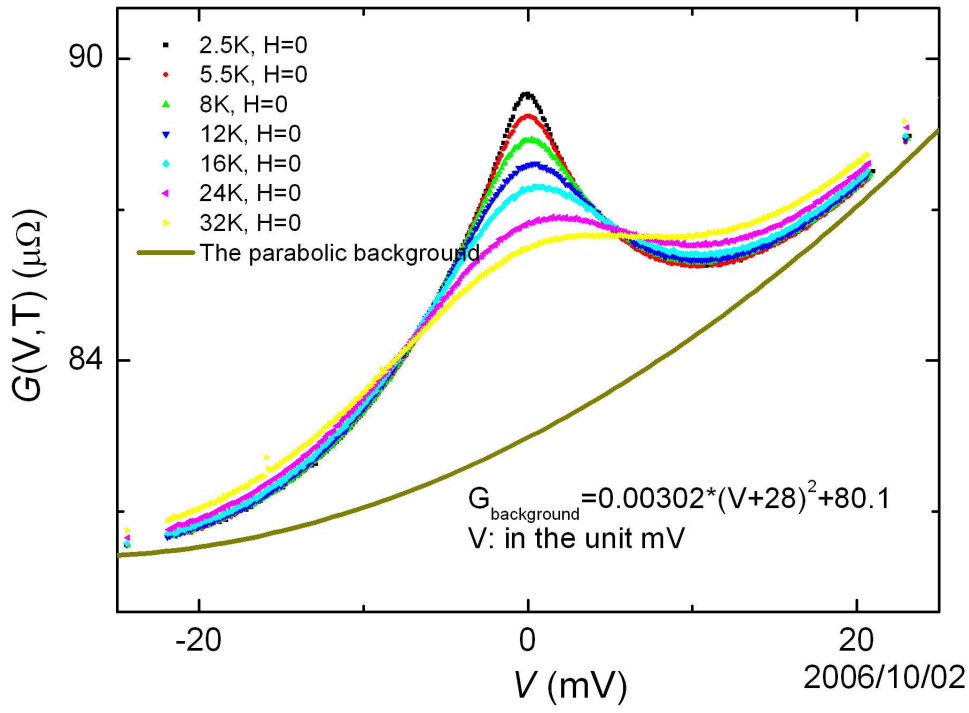

Figure 4.13: $G(V,T)$ as a function of V at several temperatures of the 20061002_Al/AlO_x/Sc tunnel junction.
The parabolic background $G_{background}(V) = 0.00302(V+28)^2 + 80.1$.

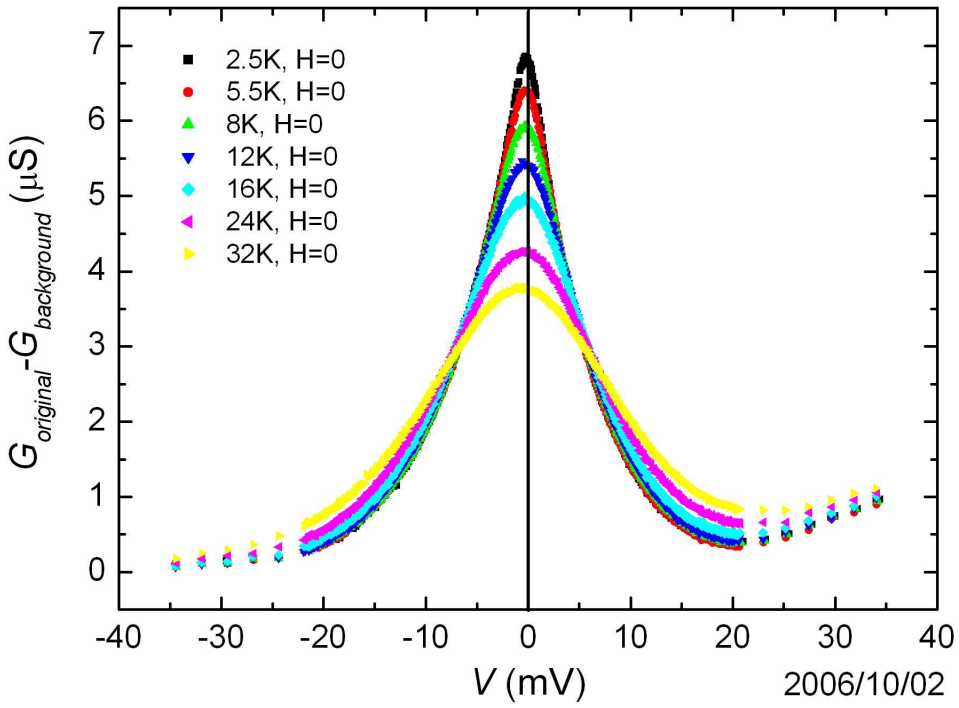

Figure 4.14: $G_{remainder}(\equiv G_{original} - G_{background})$ of the 20061002_Al/AlO_x/Sc tunnel junction.
$G_{remainder}$ is not symmetric to $V = 0$, and therefore it must contain an asymmetric term.